Pressure-induced structural and dynamical changes in liquid Si—an *ab initio* study

2006 J. Phys.: Condens. Matter 18 3591

(http://iopscience.iop.org/0953-8984/18/15/006)

INSTITUTE OF PHYSICS PUBLISHING JOURNAL OF PHYSICS: CONDENSED MATTER

J. Phys.: Condens. Matter **18** (2006) 3591–3605 doi:10.1088/0953-8984/18/15/006

Pressure-induced structural and dynamical changes in liquid Si—an *ab initio* study

A Delisle[1], **D J González**[2] **and M J Stott**[1]

[1] Department of Physics, Queen's University, Kingston, ON, Canada
[2] Departamento de Física Teórica, Universidad de Valladolid, Valladolid, Spain

Received 22 December 2005
Published 30 March 2006
Online at stacks.iop.org/JPhysCM/18/3591

Abstract

The static and dynamic properties of liquid Si at high pressure have been studied using the orbital-free *ab initio* molecular dynamics method. Four thermodynamic states at pressures of 4, 8, 14 and 24 GPa are considered, for which x-ray scattering data are available. The calculated static structure shows qualitative agreement with the available experimental data. We analyse the remarkable structural changes occurring between 8 and 14 GPa along with their effect on several dynamic properties.

1. Introduction

The intriguing properties of silicon along with its technological importance have stimulated intensive theoretical [1–9] and experimental [10–16] work. Its high-density forms include the semiconducting and covalent crystalline and amorphous phases and the metallic liquid phase. Upon melting it undergoes a semiconductor–metal transition, a density increase of $\approx$10% and significant changes in the local structure which evolves from an open one, with a tetrahedral fourfold coordination, to a liquid structure with approximately sixfold coordination. In crystalline Si (c-Si) the semiconducting diamond structure contracts with pressure and transforms at 12 GPa [17] to the metallic white-tin structure and then to the metallic simple hexagonal structure at 16 GPa [18]. The local structure of liquid Si (l-Si) at the triple point (TP) is somewhat similar to high-pressure forms of c-Si, and it has been suggested that l-Si might consist of a mixture of diamond-type and white-tin-type structures with the proportion of the latter increasing with pressure.

Within this backdrop, Funamori and Tsuji [16] have recently carried out x-ray (XR) diffraction experiments to determine the static structure of l-Si at pressures of 4, 8, 14 and 23 GPa and temperatures about 50 K above the melting point at that pressure. From an analysis of the static structure factors $S(q)$ and the associated pair distribution functions $g(r)$, Funamori and Tsuji [16] concluded that l-Si up to 8 GPa has a local structure intermediate between the diamond type and the white-tin type. But, between 8 and 14 GPa drastic structural changes were noted, with l-Si transforming to a denser structure similar to that of l-Sn at ambient pressure, as evinced by the strong similarities between the $S(q)$ values of l-Sn and l-Si at 14 GPa.

Prompted by these experimental developments, we have performed an *ab initio* molecular dynamics (AIMD) study of several static and dynamic properties of compressed l-Si at the thermodynamic states addressed by Funamori and Tsuji [16]. Of particular interest is the reflection of the reported structural changes in the dynamic properties. Our AIMD method is based on density functional theory (DFT) [19] which, for given nuclear positions, allows the calculation of the ground state electronic energy and yields the forces on the nuclei via the Hellmann–Feynman theorem, enabling MD simulations in which the nuclear positions evolve according to classical mechanics, whereas the electronic subsystem follows adiabatically. Most AIMD methods are based on the Kohn–Sham (KS) form of DFT (KS-AIMD methods) which treats the electron kinetic energy exactly, but which at present poses heavy computational demands, limiting the size of the systems to be studied as well as the simulation times. Some of these constraints can be relaxed by the so-called orbital-free *ab initio* molecular dynamics (OF-AIMD) method, which approximates the electron kinetic energy but disposes of the electronic orbitals of the KS formulation. The method allows simulations in which the number of variables describing the electronic state is greatly reduced so that larger samples (several hundreds of particles) can be studied for longer simulation times (tens of ps).

Theoretical studies of l-Si have mainly focused on static structural properties for thermodynamic states near the TP. Most studies were classical MD simulations using effective interatomic potentials constructed either empirically by fitting to experimental data [1, 2] or derived from some approximate theoretical model [3–5]. Recently, KS-AIMD calculations [6–8] have been reported which address electronic and static properties. Stich *et al* [6] and Chelikowsky *et al* [8] have reported KS-AIMD calculations for l-Si for 64 particles, using non-local pseudopotentials and the local density approximation. A subsequent calculation [7] used 350 particles and an improved treatment of electron exchange and correlation. Recently, we have carried out an OF-AIMD simulation [9] for l-Si near the TP for 2000 particles using a first principles local pseudopotential. Both static and dynamic properties were calculated with results in good agreement with the available experimental data, supporting the validity of the OF-AIMD for treating systems such as l-Si which show some remnants of covalent bonding and are not fully metallic.

On the experimental side, besides the aforementioned XR experiments of Funamori and Tsuji [16], we also quote the availability of both neutron scattering (NS) [10] and x-ray (XR) [11–13] diffraction data as well as the recent inelastic x-ray scattering (IXS) data of Hosokawa *et al* [14, 15] which have provided information on the dynamic structure of l-Si near TP.

In the next section the orbital-free *ab initio* molecular dynamics (OF-AIMD) scheme is described briefly, with emphasis on the electronic kinetic energy functional and the local pseudopotential used to characterize the electron–ion interaction. In section 3 the results of the *ab initio* simulations for several static and dynamic properties are presented and compared with the available experimental data. Finally, conclusions are drawn and ideas for further improvements are suggested.

2. Theory

The OF-AIMD method used in this study is described fully in earlier work [20], and has previously been used to study l-Si near the TP [9]. In summary, an explicit density functional for the electronic energy is minimized iteratively for each ion configuration, the forces on the ions are found using the Hellman–Feynman theorem, and the ion positions and velocities are updated by solving Newton's equations. The approximate electron kinetic energy functional which correctly gives the Thomas–Fermi and linear response limits is based on the von

Table 1. Input data for the different thermodynamic states studied in this work. ρ_i is the total ionic number density and T is the temperature, which have been taken from [16].

P (GPa)	ρ_i (Å^{-3})	T (K)
4	0.058	1503
8	0.060	1253
14	0.067	1093
23	0.071	1270

Weizsäcker term plus a correction which uses an averaged density [20]. The local electron–ion pseudopotential was constructed, for each thermodynamic state, according to the procedure described in [20].

Simulations have been performed for l-Si in the four thermodynamic states listed in table 1. These correspond to pressures of 4, 8, 14 and 23 GPa and temperatures about 50 K above the melting point for each pressure [16]. Each simulation used 2000 ions in a cubic cell with periodic boundary conditions and size appropriate for the ionic number density, ρ_i. The square root of the electron density was expanded in plane waves up to a cutoff energy $E_{\mathrm{Cut}} = 15.75$ Ryd. The Verlet leapfrog algorithm with a timestep of 3.5×10^{-3} ps was used to update the ion positions and velocities. Equilibration lasted 10 ps and the calculation of properties was made averaging over a further 65 ps. For comparison, we mention that the KS-AIMD simulations for l-Si near the TP lasted 1.2 ps [6], 0.9 ps [7] and 1.0 ps [8], which precludes its application to the study of most dynamical properties.

Several liquid static properties were evaluated during the simulation (pair distribution function, static structure factor and bond angle distribution), as well as various dynamic properties, both single-particle ones (velocity autocorrelation function, mean square displacement) and collective ones (intermediate scattering functions, dynamic structure factors, longitudinal and transverse currents). The calculation of the time correlation functions (CFs) was performed by taking time origins every five time steps. Several CFs are also dependent on the wavevector $q \equiv |\mathbf{q}|$.

3. Results

3.1. Static properties

The simulations yield directly the pair distribution function, $g(r)$, and the static structure factor $S(q)$. Figure 1 shows the calculated $S(q)$ along with the corresponding XR data of Funamori and Tsuji [16]. The experimental $S(q)$ show changes with increased pressure. The main peak grows in intensity and its position (q_{p}) increases monotonically, whereas the position of the second peak decreases between 8 and 14 GPa; the distinctive shoulder at the high-q side of the main peak shrinks smoothly and practically vanishes at 23 GPa. These changes are also reflected in $g(r)$. The position of the main peak (r_{p}), identified with the average nearest neighbour distance, decreases with pressure except for an increase between 8 and 14 GPa; the position of the second peak decreases monotonically with pressure.

These features are displayed qualitatively in the calculated $S(q)$ and $g(r)$ although there are some quantitative discrepancies with the experimental data. Figure 1 shows that the OF-AIMD $S(q)$ overestimate the intensity of the main peak and slightly underestimate the shoulder. Otherwise the positions of the peaks as well as the amplitudes of the subsequent oscillations are accounted for fairly well. A more detailed comparison with experiment is provided in table 2, which summarizes most of this structural information. This agreement

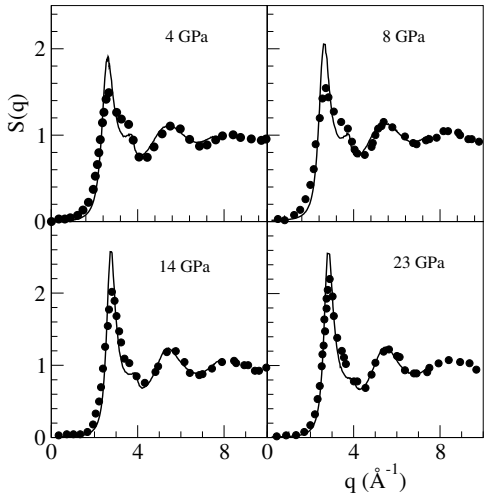

Figure 1. Static structure factor of l-Si at different high pressures. Full circles: experimental x-ray diffraction data [16]. Continuous line: OF-AIMD simulations.

Table 2. Calculated values of q_p (Å^{-1}), r_p (Å), r_m (Å) and coordination number (CN), for the different states. The numbers in parentheses are the corresponding experimental data from [16].

P (GPa)	q_p	r_p	r_m	CN	CN[a]
4	2.61 (2.67)	2.52 (2.46)	3.03	6.6 (6.8)	6.9
8	2.65 (2.72)	2.50 (2.42)	3.07	7.2 (7.1)	7.3
14	2.78 (2.82)	2.51 (2.46)	3.20	9.6 (8.5)	8.9
23	2.84 (2.88)	2.47 (2.43)	3.28	11.0 (9.2)	9.5

[a] Calculated by integrating the RDF up to $r_m = 3.1$ Å.

with experiment is similar to that achieved in earlier orbital-free simulations [9] and in KS-AIMD [6–8] calculations performed for l-Si near the TP.

Based on their experimental data for $S(q)$ and $g(r)$, Funamori and Tsuji [16] have argued that l-Si undergoes a high-pressure structural transformation between 8 and 14 GPa. Whereas l-Si contracts with pressure up to at least 8 GPa by reducing the bond length, as measured by r_p, the increase in r_p between 8 and 14 GPa suggests a structural change with an increase in the coordination number (CN). An estimate of the CN may be obtained by integrating the radial distribution function (RDF), $4\pi r^2 \rho_i g(r)$, up to the position of the first minimum, r_m, in the RDF [21, 22]. The results from the calculated RDF in table 2 show that the CN grows with compression but with an abrupt increase from 8 to 14 GPa. Funamori and Tsuji [16] obtained CN values, also given in table 2, by integrating their experimental RDF up to 3.1 Å for all the states, and a similar growth between 8 and 14 GPa is seen. Had we used the same $r_m = 3.1$ Å as Funamori and Tsuji did for calculating the CN, then the agreement with the 'experimental' values would have been even better, but taking r_m as the position of the first minimum is thought to be more soundly based.

Values for the isothermal compressibility, κ_T, have been obtained from $S(0) = \rho_i k_B T \kappa_T$ by using a least-squares fit to calculate the $S(q)$ for q-values up to 0.8 Å^{-1} and extrapolating to $q \to 0$. The results are given in table 3. Although no experimental results are available, the OF-AIMD calculation for l-Si near the TP yielded $\kappa_T = 3.0$, which is rather close to the experimental value [23] of 2.8 (in 10^{-11} m^2 Nw^{-1} units).

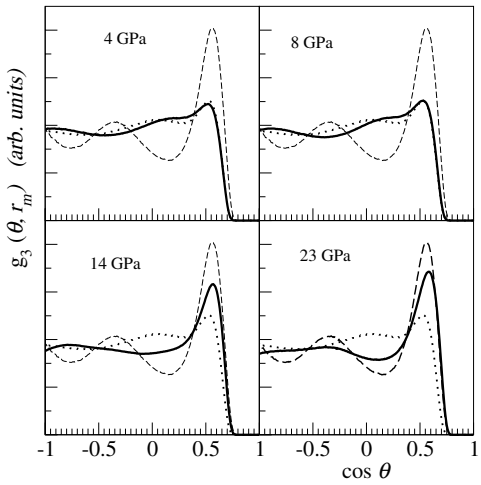

Figure 2. Bond-angle distribution function, $g_3(\theta, r_m)$, of l-Si at different high pressures (full line). The dotted and dashed lines stand respectively for l-Si and l-Al at their respective TPs.

Table 3. Calculated values of $S(q \to 0)$, isothermal compressibility κ_T (in 10^{-11} m^2 Nw^{-1} units) and adiabatic sound velocity (c_s) for the different states.

P (GPa)	$S(q \to 0)$	κ_T (10^{-11} m^2 Nw^{-1})	c_s (m s^{-1})
4	0.0180 ± 0.003	1.50 ± 0.3	5100
8	0.0135 ± 0.003	1.30 ± 0.3	5400
14	0.0095 ± 0.003	0.94 ± 0.3	6300
23	0.0085 ± 0.003	0.68 ± 0.3	6750

Further structural information is provided by higher-order correlation functions such as the bond-angle distribution function, $g_3(\theta, r_m)$, where θ is the angle between two vectors joining a reference particle with two neighbouring particles at a distance less than r_m. In a simple liquid metal such as Al, $g_3(\theta, r_m)$ has peaks at around $\theta \approx 60°$ and 120°, which are close to those expected for a local icosahedral arrangement [24] ($\theta \approx 63.5°$ and 116.5°). In contrast, for l-Si near the TP both the OF-AIMD [9] and KS-AIMD [6–8] calculations for $g_3(\theta, r_m)$ have yielded two maxima centred around $\theta \approx 60°$ and 89°. This double-peak feature has been interpreted as a manifestation of tetrahedral bonding and higher coordinated atoms both contributing to the first coordination shell. In illustration, figure 2 shows the OF-AIMD results for the $g_3(\theta, r_m)$ of l-Si and l-Al near their TPs [9, 20]. OF-AIMD results for compressed l-Si are also included in the figure, and a gradual evolution with pressure towards the simple liquid metal distribution is seen. There is little change up to 8 GPa although the wide maximum at $\theta \approx 89°$ has moved to slightly smaller θ-values, which may indicate less tetrahedral bonding. But, as the pressure increases from 8 to 14 GPa, there is a qualitative change in $g_3(\theta, r_m)$, whose shape moves closer to that of the simple liquid metals, and at 23 GPa the positions of the maxima for l-Si and l-Al are rather similar.

3.2. Dynamic properties

3.2.1. Collective dynamics. The intermediate scattering function, $F(q, t)$, contains both spatial and temporal information on the collective dynamics of density fluctuations. It is defined

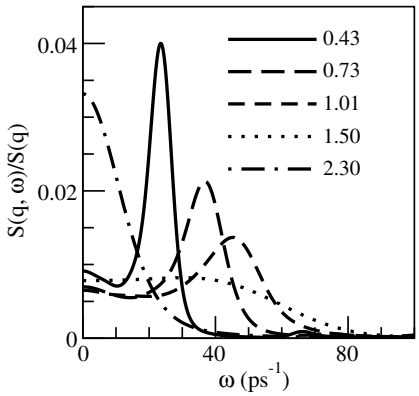

Figure 3. Dynamic structure factor $S(q, \omega)$ at several q-values (in Å^{-1} units), for l-Si at 8 GPa.

as

$$F(q,t) = \frac{1}{N}\left\langle \left(\sum_{m=1}^{N} \mathrm{e}^{-\mathrm{i}\vec{q}\,\vec{R}_{\mathrm{m}}(t+t_0)}\right)\left(\sum_{l=1}^{N} \mathrm{e}^{\mathrm{i}\vec{q}\,\vec{R}_{\mathrm{l}}(t_0)}\right)\right\rangle. \tag{1}$$

Its frequency spectrum is the dynamic structure factor, $S(q, \omega)$, which has experimental relevance due to its connection with the scattered intensity in inelastic x-ray or neutron experiments. The calculated $F(q, t)$ for compressed l-Si exhibit an oscillatory behaviour up to $q \approx (3/5)q_{\mathrm{p}}$, with the amplitude diminishing for larger q-values. This oscillatory behaviour is typical of simple liquid metals found by either computer simulation [20, 25–27] or from theoretical models [28], and gives rise to a well-defined inelastic peak in $S(q, \omega)$.

The $S(q, \omega)$, obtained by a time Fourier transform (FT) of $F(q, t)$, exhibit, for all the states, well-defined sidepeaks which are indicative of collective density excitations. This is illustrated in figure 3, which shows calculated $S(q, \omega)$ for l-Si at 8 GPa for several q-values. The general shape of $S(q, \omega)$ is qualitatively similar at equivalent q/q_{p}-values for all the compressed states, and no specific feature of $S(q, \omega)$ has been identified whose variation would mark the structural transformation occurring somewhere between 8 and 14 GPa.

For all the states the sidepeaks in $S(q, \omega)$ persist up to $q \approx (3/5)q_{\mathrm{p}}$, which is a feature shared by both l-Si [9] and the simple liquid metals near their TPs [20, 24]. The dispersion relations, $\omega_{\mathrm{m}}(q)$, of the density fluctuations have been obtained from the positions of these sidepeaks. They are plotted in figure 4 for the 8, 14 and 23 GPa states together with the calculated OF-AIMD [9] results and experimental data [14] for l-Si near its TP. The curves look qualitatively similar but there is a marked difference between $\omega_{\mathrm{m}}(q)$ for 8 GPa and less, and those for 14 and 23 GPa. In addition, the slope of the dispersion gives a q-dependent adiabatic sound velocity, $c_{\mathrm{s}}(q)$, which in the limit $q \to 0$ reduces to the bulk adiabatic sound velocity, c_{s}. This has been estimated by fitting a straight line to the low-q region of the $\omega_{\mathrm{m}}(q)$, and the results are given in table 3. The c_{s} increase with pressure but a steeper rise from 8 to 14 GPa will be seen.

The transverse current correlation function, $J_{\mathrm{t}}(q, t)$, provides information on shear modes and is not directly related to any measurable quantity. It can only be obtained from either theoretical models or computer simulations, but it is known that its shape evolves from a Gaussian, in both q and t, at the free particle ($q \to \infty$) limit, towards a Gaussian in q and an exponential in t in the hydrodynamic limit ($q \to 0$), i.e.,

$$J_{\mathrm{t}}(q \to 0, t) = \frac{1}{\beta m}\mathrm{e}^{-q^2\eta|t|/m\rho_i}, \tag{2}$$

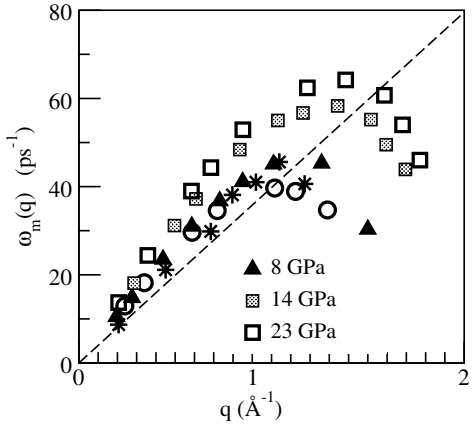

Figure 4. Dispersion relation for the peak positions, $\omega_m(q)$, from the calculated $S(q, \omega)$, for l-Si at different high pressures. The figure also includes the calculated (open circles) [9] and experimental (asterisks) [14] results for l-Si near the triple point ($T = 1740$ K). Dashed line: linear dispersion with the hydrodynamic sound velocity, $v = 3977$ m s^{-1}, at the triple point.

where η is the shear viscosity coefficient, $\beta = (k_B T)^{-1}$ and m is the atomic mass. In both small and large q limits, $J_t(q, t)$ is always positive, but for intermediate q-values there is a more complicated behaviour with well-defined oscillations [20, 24, 29]. Calculated $J_t(q, t)$ for several q-values are shown in figures 5 and 6 for l-Si at 8 and 14 GPa respectively. The most noteworthy effect on $J_t(q, t)$ of an increasing pressure is reflected in the oscillations, which have a smaller amplitude and last for appreciably shorter times at the lower pressures. Its consequences are apparent in the frequency spectra, $J_t(q, \omega)$, which are plotted in the lower panels of figures 5 and 6. For both 14 and 23 GPa the $J_t(q, \omega)$ exhibits an inelastic peak which appears at low q-values ($\approx$0.45 Å^{-1}) and persists up to about $q = 2.50$ Å^{-1}. However, for 8 GPa the inelastic peaks appear for a appreciably smaller range (0.85 Å$^{-1} \leqslant q \leqslant 1.50$ Å^{-1}) while for 4 GPa there are no inelastic peaks. This absence of peaks in $J_t(q, \omega)$ is also a feature of l-Si near the TP, but is at variance with the behaviour of a large number of different liquids such as hard sphere systems [29], Lennard-Jones liquids [24, 29] and simple liquid metals [20, 24, 27] near melting, for which $J_t(q, t)$ oscillates and the associated $J_t(q, \omega)$, has an inelastic peak over some range of q-values. The inelastic peak in $J_t(q, \omega)$ is associated with propagating shear waves which seem to be absent in l-Si up to somewhere between 4 and 8 GPa. However, it must be noted that whereas in simple liquid metals near melting the shear waves last up to $q \approx 3q_p$, in the case of l-Si at 14 and 23 GPa they appear up to $q \approx 0.9q_p$.

The shear viscosity coefficient, η, can be calculated from $J_t(q, t)$ using the memory function representation [20, 30, 31]

$$\tilde{J}_t(q, z) = \frac{1}{\beta m}\left[z + \frac{q^2}{\rho_i m}\tilde{\eta}(q, z)\right]^{-1}, \tag{3}$$

where the tilde denotes the Laplace transform, and $\tilde{\eta}(q, z)$ is a generalized shear viscosity coefficient. The $\int_0^\infty dt\, J_t(q, t)$ when normalized gives $\beta m \tilde{J}_t(q, z = 0)$, from which $\tilde{\eta}(q, z = 0)$ are obtained and extrapolated to $q = 0$ to give the usual shear viscosity coefficient, η. Results are given in table 4. Although no comparison can be made with experimental results, the calculated values are considered reliable because the application of this approach to l-Si near its TP gave $\eta = 0.75 \pm 0.15$ GPa ps, in reasonable agreement with the available experimental

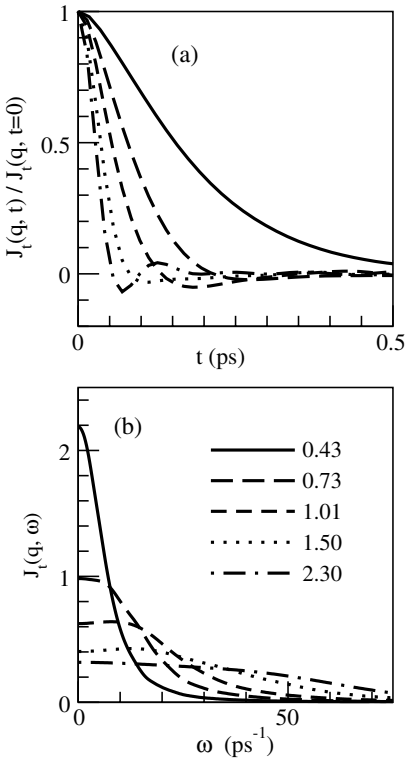

Figure 5. (a) Transverse current correlation function $J_t(q,t)$ at several q-values (in Å^{-1} units), for l-Si at 8 GPa. (b) The same for $J_t(q,\omega)$.

data [32], $\eta_{exp} = 0.58$–0.78 GPa ps. It is noteworthy that once more η undergoes an abrupt change as the pressure increases from 8 to 14 GPa.

3.2.2. Single-particle dynamics. Information about the single-particle properties is contained in the self-intermediate scattering function

$$F_s(q,t) = \frac{1}{N}\left\langle \sum_{j=1}^{N} e^{-i\vec{q}\vec{R}_j(t+t_0)} e^{i\vec{q}\vec{R}_j(t_0)} \right\rangle \tag{4}$$

and its frequency spectrum, the self-dynamic structure factor, $S_s(q,\omega)$, which is related to the incoherent part of the total intensity scattered in an INS experiment. The OF-AIMD results for the $F_s(q,t)$ presented in figure 7 for two states display the usual monotonic decay with time, and comparison of different states shows that at similar q/q_p-values $F_s(q,t)$ decays slower with increasing pressure, with the 14 and 23 GPa states behaving very much like the liquid simple metals [20, 24, 28] near their TPs. The different rates of decay can be related to the differences in the self-diffusion coefficients.

Closely related to $F_s(q,t)$ is the velocity autocorrelation function (VACF) of a tagged ion in the fluid, $Z(t)$, which can be obtained as the $q \to 0$ limit of the first-order memory function of the $F_s(q,t)$, but more conveniently, from its definition

$$Z(t) = \langle \vec{v}_1(t)\vec{v}_1(0)\rangle / \langle v_1^2 \rangle. \tag{5}$$

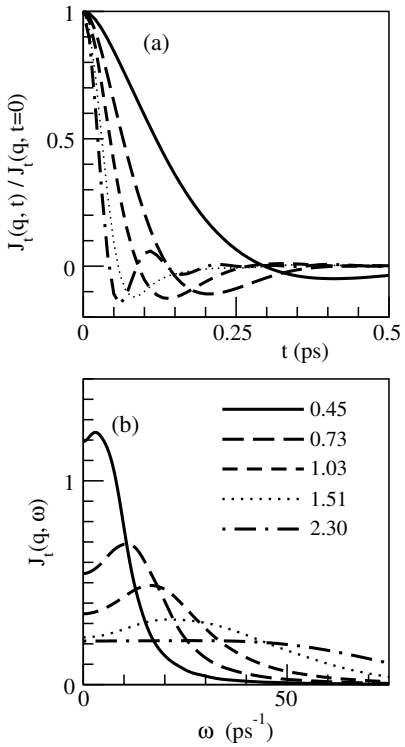

Figure 6. (a) Transverse current correlation function $J_t(q, t)$ at several q-values (in Å^{-1} units), for l-Si at 14 GPa. (b) The same for $J_t(q, \omega)$.

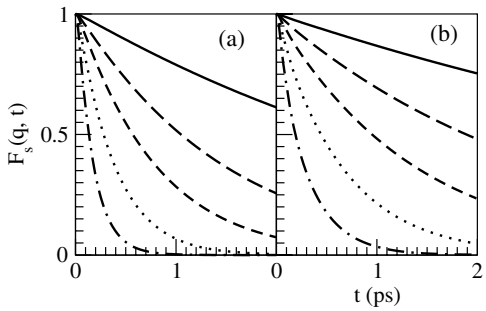

Figure 7. Self intermediate scattering functions, $F_s(q, t)$, at several q-values (in Å^{-1} units), for l-Si at (a) 8 GPa and (b) 14 GPa. The key for the symbols is the same as in the previous figure.

Figures 8 and 9 show results for $Z(t)$ and for its power spectrum $Z(\omega)$. The overall shape of $Z(t)$ changes little from the TP up to 8 GPa, but as the pressure is further increased changes occur in the range and amplitude of the oscillations until at 23 GPa the shape is very similar to that of the simple liquid metals at their TPs. These changes can be explained in terms of the so-called 'cage' effect due to backscattering from the shell of nearest neighbours reversing the initial velocity of a tagged ion and driving a deeper first minimum. This is consistent with the results for the static structure, summarized in table 2, which shows an open structure up to 8 GPa but a marked increase in the coordination number at higher pressures.

Table 4. Calculated values of the self-diffusion (D) and shear viscosity η (in GPa ps) for the different states.

P (GPa)	D (Å^2 ps^{-1})	η (GPa ps)
4	1.82 ± 0.05	0.77 ± 0.10
8	1.33 ± 0.05	0.84 ± 0.10
14	0.70 ± 0.03	1.47 ± 0.15
23	0.70 ± 0.03	1.55 ± 0.15

The power spectra which are plotted in figure 9 also show significant changes between 8 and 14 GPa. $Z(\omega)$ evolves with pressure from a shape resembling l-Si near the TP towards a liquid simple metal shape with a low-frequency peak and a higher-frequency peak (or shoulder) [20, 24]. The shoulder at $\omega \approx 40$ ps^{-1}, present at all the pressures, has been related to vibrational remnants in the liquid of the covalent bonding [6]. Below 8 GPa, low-frequency diffusive modes are present.

The self-diffusion coefficient, D, is readily obtained from either the time integral of $Z(t)$ or from the slope of the mean square displacement $\delta R^2(t) \equiv \langle |\vec{R}_1(t) - \vec{R}_1(0)|^2 \rangle$ of a tagged ion in the fluid, as follows:

$$D = \frac{1}{\beta m} \int_0^\infty Z(t)\, \mathrm{d}t; \qquad D = \lim_{t\to\infty} \delta R^2(t)/6t. \tag{6}$$

Both routes for D lead to practically the same value, and the results are given in table 4. The decreasing value of D with increasing pressure is due to the growing importance of backscattering. No experimental results are available for the diffusion coefficients of l-Si, but confidence in the results may be taken from the agreement between the OF-AIMD result for l-Si near the TP: $D_{\text{OF-AIMD}} = 2.28$ Å^2 ps^{-1}, and the estimates from KS-AIMD calculations of Stich *et al* [6, 7]: $D_{\text{KS-AIMD}} = 2.02$ Å^2 ps^{-1} [6] which slightly increased to 2.4 Å^2 ps^{-1} [7] when the number of particles was augmented to 350 particles. Another KS-AIMD study by Chelikowsky *et al* [8] has yielded $D_{\text{KS-AIMD}} = 1.90$ Å^2 ps^{-1}. The results for D at 4 and 8 GPa are similar to the value at the l-Si TP, whereas the results for 14 and 23 GPa are closer to those for the liquid simple metals near their TPs [20, 33, 34]. This change in D with pressure explains the different decay rates found in the $F_s(q, t)$ which decayed much faster at the lower pressures. Recalling the accurate Gaussian approximation [24, 29], $F_s(q, t) = \exp[-q^2 \delta R^2(t)/6]$, it will be seen that a greater D implies a greater $\delta R^2(t)$ and therefore a faster decay of $F_s(q, t)$.

The self-diffusion coefficient, D, of a macroscopic particle of diameter d undergoing Brownian motion in a liquid of viscosity η is related to η through the Stokes–Einstein (SE) relation $\eta D = k_B T/2\pi d$. This relation has often been used on an atomic scale to estimate η by identifying d with the position, r_p, of the main peak in $g(r)$. Using the D values for 4, 8, 14 and 23 GPa the relation yields $\eta = 0.72$, 0.82, 1.36 and 1.59 GPa ps respectively, values rather close to the earlier OF-AIMD estimates.

Gaskell and Miller [35] have used mode-coupling (MC) theory to develop a representation of the normalized VACF which has been used to interpret MD data in various fluids [35–37], and which sheds light on l-Si. Within this approach

$$Z(t) \approx \frac{1}{24\pi^3} \int \mathrm{d}\mathbf{q}\, f(q)[J_l(q, t) + 2J_t(q, t)]F_s(q, t) \equiv Z_l(t) + Z_t(t) \tag{7}$$

where $J_l(q, t)$ and $J_t(q, t)$ are the normalized longitudinal and transverse current correlation functions and $f(q)$ is

$$f(q) = \frac{3}{\rho_i} \frac{j_1(aq)}{aq} \tag{8}$$

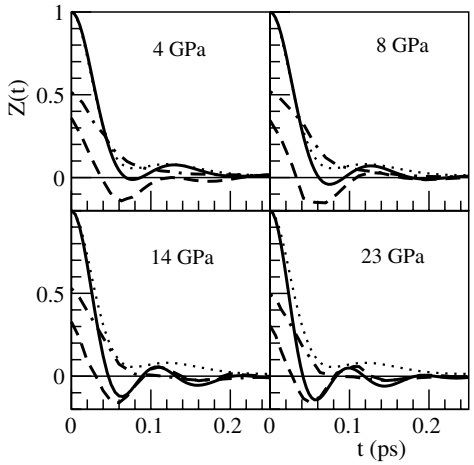

Figure 8. Full line: normalized velocity autocorrelation function $Z(t)$ for l-Si at different pressures. The dashed and dash–dotted lines stand for the respective longitudinal, $Z_{\mathrm{l}}(t)$, and transverse, $Z_{\mathrm{t}}(t)$, components as defined in equation (7). The dotted line depicts the result for l-Si at the triple point ($T = 1740$ K).

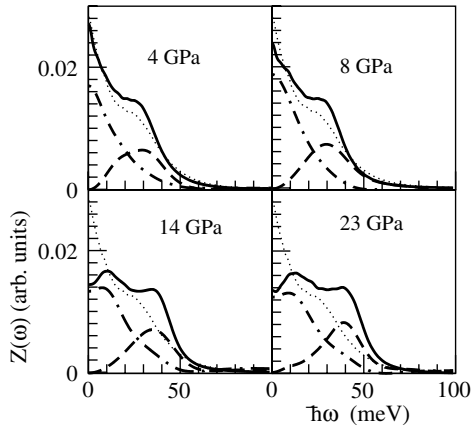

Figure 9. Power spectrum, $Z(\omega)$, for l-Si at different pressures. The dashed and dash–dotted lines stand for the respective longitudinal, $Z_{\mathrm{l}}(\omega)$, and transverse, $Z_{\mathrm{t}}(\omega)$, components. The dotted line depicts the result for l-Si at the triple point ($T = 1740$ K).

with $j_1(x)$ the spherical Bessel function of order one; ρ_i is the ion number density and $a = (3/4\pi\rho_i)^{1/3}$ is the radius per ion. Substitution into equation (7) of the OF-AIMD results for $J_{\mathrm{l}}(q,t)$, $J_{\mathrm{t}}(q,t)$ and $F_{\mathrm{s}}(q,t)$ allows identification of longitudinal and transverse current contributions, $Z_{\mathrm{l}}(t)$ and $Z_{\mathrm{t}}(t)$, respectively. The two contributions are plotted in figure 8 which shows that the oscillatory behaviour in the $Z(t)$ is due to $Z_{\mathrm{l}}(t)$, but again the step from 8 to 14 GPa changes the shape of both contributions. Up to 8 GPa, $Z_{\mathrm{t}}(t)$ remains positive for all times as a result of the positive nature of $J_{\mathrm{t}}(q,t)$ (see figures 5 and 6) and determines the long time behaviour of the $Z(t)$; however, from 14 GPa on, $Z_{\mathrm{t}}(t)$ develops a shallow and broad negative minimum centred at rather long times $\approx$0.15 ps. On the other hand, $Z_{\mathrm{l}}(t)$ accounts for most of the backscattering effect. With higher pressure the first minimum sharpens and moves to shorter times and the oscillations extend further, which are results of the increasing role of

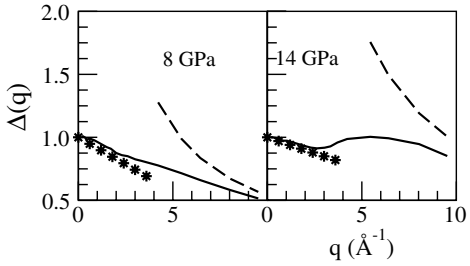

Figure 10. Normalized HWHM of $S_s(q, \omega)$, relative to its value at the hydrodynamic limit, for l-Si at 8 and 14 GPa. Continuous line: OF-AIMD results. Asterisks: mode-coupling theory. Dashed line: free-particle limit.

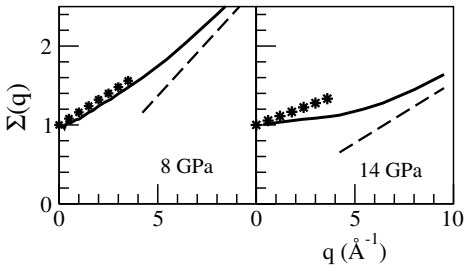

Figure 11. Same as figure 10, but for the normalized peak value $S_s(q, \omega = 0)$, relative to its value at the hydrodynamic limit.

the 'cage' effect. At 14 and 23 GPa, both components are similar in shape to their liquid simple metal counterparts [35] with both oscillating about zero and with $Z_l(t)$ controlling the large-t behaviour of $Z(t)$. Finally, notice that the development of the deep minimum in the $Z(t)$ is mainly due to the rapid decay of $Z_t(t)$ with increasing pressure.

The longitudinal and transverse components of the power spectrum, $Z(\omega)$, are shown in figure 9. The spectrum at small ω is dominated by $Z_t(\omega)$, and, consequently, the diffusion constant $D \propto Z(\omega = 0)$ is completely determined by the transverse component. For 4 and 8 GPa, $Z_t(\omega)$ decreases monotonically, but at 14 and 23 GPa the value at zero frequency has dropped and a low-frequency peak has developed. Note that $Z_t(\omega)$ has no maximum for 4 and 8 GPa, which are the states where $J_t(q, \omega)$ shows either no inelastic peaks (4 GPa) or they exist for a small range (8 GPa). The longitudinal component $Z_l(\omega)$ always exhibits a peak whose position increases slightly with increasing pressure. This peak is responsible for the shoulder in the total $Z(\omega)$ for the 4 and 8 GPa states, as well as for the high-frequency peak for the 14 and 23 GPa states.

By a time FT of the $F_s(q, t)$ we obtain its frequency spectrum, $S_s(q, \omega)$, which is known as the self-dynamic structure factor and is related to the incoherent part of the measured INS cross-section. For all q-values $S_s(q, \omega)$ decays monotonically as a function of frequency and it can be characterized in terms of the peak value, $S_s(q, \omega = 0)$, and the HWHM, $\omega_{1/2}(q)$. These parameters are frequently reported normalized with respect to the hydrodynamic ($q \to 0$) limit, by introducing the dimensionless quantities $\Sigma(q) = \pi q^2 D S_s(q, \omega = 0)$ and $\Delta(q) = \omega_{1/2}(q)/q^2 D$, where $\omega_{1/2}(q)/q^2$ can be interpreted as an effective q-dependent diffusion coefficient $D(q)$. For a simple liquid near its TP, $\Delta(q)$ usually oscillates, whereas in a dense gas it decreases monotonically from unity at $q = 0$ to the $1/q$-behaviour at large q [24, 25, 29]. Figures 10 and 11 depict the OF-AIMD results for $\Delta(q)$ and $\Sigma(q)$ for 8 and 14 GPa, as this

is the pressure range where both magnitudes undergo a substantive change. The obtained $\Delta(q)$ for 14 GPa shows an oscillatory shape with a minimum located at $q \approx q_p$ which can be traced back to structural features ('cage' effect) which somewhat hinder the motion of the ions and become more effective at $q \approx q_p$ where the wavelength is comparable to the size of the cage. Conversely, that for 8 GPa resembles the situation of a dense gas where the 'cage' effect becomes negligible, leading to a net reduction of the diffusion coefficient [24, 38] and the corresponding $\Sigma(q)$ stands very close to that of the dense gas.

An additional check on the reliability of these results may be provided by the MC theory [39, 40] which has already shown its capability to describe to experimental data for $\Delta(q)$ and $\Sigma(q)$ in simple liquid metals [38, 41] at $q \leqslant q_p$. Specifically, the MC theory avers that at low-q values

$$\begin{aligned} \Delta(q) &= 1 + H(\delta)q/q^* \\ \Sigma(q) &= 1 + G(\delta^{-1})q/q^* \end{aligned} \tag{9}$$

where $q^* = 16\pi m\rho_i\beta D^2$, $\delta = D/(D + \eta/m\rho_i)$ and $H(\delta)$ and $G(\delta^{-1})$ are given in [38].

The first term in equations (9) stands for the hydrodynamic result whereas the second one accounts for the coupling of mass diffusion and collective modes. Calculated values of D and η have been used with equations (9) to obtain the points in figures 10–11. For $q \leqslant q_p$ we observe that the MC theory fairly accounts for the OF-AIMD results, with an accuracy comparable to what has already been achieved in other liquid metals [38]. Consequently, the present results show the ability of the MC theory to describe the single particle dynamics (and presumably the collective dynamics too) in liquid systems encompassing a range of bonding and structure such as that displayed by the compressed l-Si.

4. Conclusions

Several static and dynamic properties of l-Si at four high-pressure thermodynamic states have been investigated using orbital-free *ab initio* molecular dynamics combined with a first-principles local pseudopotential.

The study was motivated by experimental findings [16] of significant structural changes in l-Si when the pressure is increased from 4 to 23 GPa. The obtained results for the static structure qualitatively follow those trends unveiled by the experiment, namely the increase of the intensity and the position of the $S(q)$'s main peak, along with a progressive vanishing of its shoulder. Other parameters such as the coordination number, isothermal compressibility, and the shape of the bond-angle distribution function provide further insight into the changes. Overall, apart from a contraction with increasing pressure, the static structures of l-Si at the TP, and at 4 and 8 GPa are very similar. Above 8 GPa the system transforms to a denser more close-packed structure typical of a liquid simple metal, with most change taking place between 8 and 14 GPa.

The structural changes are also reflected in several dynamical properties. The calculated dynamic structure factors, $S(q, \omega)$, show collective density excitations over similar wavelength ranges, namely up to $q \approx (3/5)q_p$, as those found for simple liquid metals at their TPs. These density excitations are sound waves whose velocity increases with pressure, most steeply between 8 and 14 GPa. The dispersion relations of the excitations divide into two groups, one for l-Si at its TP, 4 GPa and 8 GPa and another group for l-Si at 14 and 23 GPa.

The transverse current correlation also show evidence of the structural changes. Below 4 GPa, its frequency spectra lack inelastic peaks, indicating the absence of shear waves, but at 8 GPa clear inelastic peaks are already evident.

The calculated self-diffusion and shear viscosity transport coefficients are also affected by the structural changes occurring between 8 and 14 GPa. These transport coefficients cannot be compared with experiment, but confidence in the calculated values is given by the good agreement with experimental values and/or other *ab initio* results for l-Si and its TP.

Finally, we remark that the present results for the static and dynamic properties of compressed l-Si underscore the capability of the OF-AIMD method to tackle liquid systems encompassing a range of bonding and structure which evolves from mild remnants of covalent bonding to a metallic one. Moreover, further improvements in the present *ab initio* method are still possible and they necessarily will be focused on developing more accurate electron kinetic energy functionals and local ionic pseudopotentials.

Acknowledgments

This work has been supported by the MEC of Spain (MAT2005-03415) and the NSERC of Canada. DJG acknowledges additional financial support from the Physics Department of Queen's University, where part of this work was carried out.

References

[1] Stillinger F H and Weber T A 1985 *Phys. Rev.* B **31** 5262
Broughton J Q and Li X P 1987 *Phys. Rev.* B **35** 9120
[2] Tersoff J 1988 *Phys. Rev.* B **38** 9902
[3] Jank W and Hafner J 1990 *Phys. Rev.* B **41** 1497
[4] Wang C, Chan C and Ho K 1991 *Phys. Rev. Lett.* **66** 189
Wang C, Chan C and Ho K 1991 *Phys. Rev.* B **45** 12227
[5] Virkkunen R, Laasonen K and Nieminen R M 1991 *J. Phys.: Condens. Matter* **3** 7455
[6] Stich I, Car R and Parrinello M 1989 *Phys. Rev. Lett.* **63** 2240
Stich I, Car R and Parrinello M 1991 *Phys. Rev.* B **44** 4262
[7] Stich I, Parrinello M and Hollender J M 1996 *Phys. Rev. Lett.* **76** 2077
[8] Godlevsky V, Chelikowsky J and Troullier N 1995 *Phys. Rev.* B **52** 13281
[9] Delisle A, González D J and Stott M J 2006 *Phys. Rev.* B **73** 064202
[10] Gabathuler J P and Steeb S 1979 *Z. Naturf.* a **34** 1314
[11] Waseda Y and Suzuki K 1975 *Z. Phys.* B **20** 339
Waseda Y 1980 *The Structure of Non-Crystalline Materials* (New York: McGraw-Hill)
[12] Waseda Y, Shinoda K, Sugiyama K, Takeda S, Terashima K and Toguri J M 1995 *Japan. J. Appl. Phys.* **34** 4124
[13] Takeda S 1995 *Japan. J. Appl. Phys.* **34** 4889
[14] Hosokawa S, Greif J, Demmel F and Pilgrim W C 2003 *Nucl. Instrum. Methods Phys. Res.* B **199** 161
[15] Hosokawa S, Pilgrim W C, Kawakita Y, Ohshima K, Takeda S, Ishikawa D, Tsutsui S, Tanaka Y and Baron A Q R 2003 *J. Phys.: Condens. Matter* **15** L623
[16] Funamori N and Tsuji K 2002 *Phys. Rev. Lett.* **88** 255508
[17] Jamieson J C 1963 *Science* **139** 762
[18] Olijnyk H, Sikka S K and Holzapfel W B 1984 *Phys. Lett.* A **103** 137
Hu J Z and Spain I L 1984 *Solid State Commun.* **51** 263
[19] Hohenberg P and Kohn W 1964 *Phys. Rev.* **136** 864
Kohn W and Sham L J 1965 *Phys. Rev.* **140** A1133
[20] González D J, González L E, López J M and Stott M J 2002 *Phys. Rev.* B **65** 184201
[21] Cusak N E 1987 *The Physics of Structurally Disordered Matter* (Bristol: Hilger)
[22] McGreevy R L, Baranyai A and Ruff I 1986 *Phys. Chem. Liq.* **16** 47
[23] Baidov V V and Gitis M B 1970 *Fiz. Tekh. Poluprov.* **4** 967
Baidov V V and Gitis M B 1970 *Sov. Phys.—Semicond.* **4** 825 (Engl. Transl.)
[24] Balucani U and Zoppi M 1994 *Dynamics of the Liquid State* (Oxford: Clarendon)
Hansen J P and McDonald I R 1986 *Theory of Simple Liquids* (London: Academic)
[25] Torcini A, Balucani U, de Jong P H K and Verkerk P 1995 *Phys. Rev.* E **51** 3126
[26] Shimojo F, Hoshino K and Watabe M 1994 *J. Phys. Soc. Japan* **63** 141

[27] Kambayashi S and Kahl G 1992 *Phys. Rev.* A **46** 3255
Kahl G and Kambayashi S 1994 *J. Phys.: Condens. Matter* **6** 10897
[28] Casas J, González D J and González L E 1999 *Phys. Rev.* B **60** 10094
Casas J, González D J, González L E, Alemany M M G and Gallego L J 2000 *Phys. Rev.* B **62** 12095
[29] Boon J P and Yip S 1991 *Molecular Hydrodynamics* (New York: Dover)
[30] Palmer B J 1994 *Phys. Rev.* E **49** 359
[31] Balucani U, Brodholt J P, Jedlovszky P and Vallauri R 2000 *Phys. Rev.* E **62** 2971
[32] Sasaki H, Tokizaki E, Huang X M, Terashima K and Kimura S 1995 *Japan. J. Appl. Phys.* **34** 3432
Kimura S and Terashima K 1997 *J. Cryst. Growth* **180** 323
[33] Iida T and Guthrie R I L 1988 *Physical Properties of Liquid Metals* (Oxford: Clarendon)
[34] Alemany M M G, Casas J, Rey C, González L E and Gallego L J 1997 *Phys. Rev.* E **56** 6818
[35] Gaskell T and Miller S 1978 *J. Phys. C: Solid State Phys.* **11** 3749
Gaskell T and Miller S 1978 *J. Phys. C: Solid State Phys.* **11** 4839
Gaskell T and Miller S 1978 *Phys. Lett.* A **66** 307
[36] Barrat J L, Hansen J P and Totsuji H 1988 *J. Phys. C: Solid State Phys.* **21** 4511
[37] Balucani U, Brodholt J P and Vallauri R 1996 *J. Phys.: Condens. Matter* **8** 6139
[38] Montfrooy W, de Schepper I, Bosse J, Glaser W and Morkel Ch 1986 *Phys. Rev.* A **33** 1405
[39] Sjögren L 1980 *J. Phys. C: Solid State Phys.* **13** 705
Sjögren L 1980 *Phys. Rev.* A **22** 2866
Sjögren L 1980 *Phys. Rev.* A **22** 2883
[40] Wahnström G and Sjögren L 1982 *J. Phys. C: Solid State Phys.* **15** 401
[41] Cabrillo C, Bermejo F J, Alvarez M, Verkerk P, Maira-Vidal A, Bennington S M and Martin D 2002 *Phys. Rev. Lett.* **89** 075508
Cabrillo C, Bermejo F J, Alvarez M, Verkerk P, Maira-Vidal A, Bennington S M and Martin D 2004 *J. Phys.: Condens. Matter* **16** S309